Magnetic interactions in the $MnFe_{1-x}Co_xP$ series of solid solutions

2007 J. Phys.: Condens. Matter 19 376201

(http://iopscience.iop.org/0953-8984/19/37/376201)

IOP PUBLISHING JOURNAL OF PHYSICS: CONDENSED MATTER

J. Phys.: Condens. Matter **19** (2007) 376201 (16pp) doi:10.1088/0953-8984/19/37/376201

Magnetic interactions in the $MnFe_{1-x}Co_xP$ series of solid solutions

R Zach[1,5], J Tobola[2], B Średniawa[1], S Kaprzyk[2], M Guillot[3], D Fruchart[4] and P Wolfers[4]

[1] Institute of Physics, Cracow University of Technology, Podchorążych 1, 30 084 Cracow, Poland
[2] Faculty of Physics and Applied Computer Science, AGH University of Science and Technology, Al. Mickiewicza 30, 30-059 Cracow, Poland
[3] Laboratoire Magnetiques Champs Intences, CNRS, Av. des Martyrs, BP 166X, 38 042 Grenoble, France
[4] Laboratoire de Cristallographie, CNRS, BP 166, 38042 Grenoble cedex 9, France

E-mail: puzach@cyf-kr.edu.pl

Received 1 February 2007
Published 22 August 2007
Online at stacks.iop.org/JPhysCM/19/376201

Abstract

In this report the results of crystal structure investigations, high magnetic field measurements and electronic structure calculations carried out for the $MnFe_{1-x}Co_xP$ system are presented. The crystal structure parameters were determined using the x-ray powder diffraction method. On this basis the inter-atomic distances were calculated and the magnetic couplings between magnetic atoms in $MnFe_{1-x}Co_xP$ are discussed. Magnetic properties of the series of compounds with $x = 0.3$, 0.45, 0.5, 0.525, 0.55, 0.65 and 0.7, as determined under strong magnetic field (up to 20 T), are reported. The electronic band structure calculations were performed using the Korringa–Kohn–Rostoker method with the coherent potential approximation (KKR-CPA). The site preference of Co and Fe atoms, located in pyramidal and tetrahedral positions, was analysed and magnetic properties of Co and Fe sublattices were calculated based on total energy computations. The site-decomposed densities of states and the magnetic moment values were calculated in the whole alloy concentration range assuming a ferromagnetic (F) order. For $MnFe_{0.35}Co_{0.65}P$ the KKR-CPA calculations were carried out assuming different types of antiferromagnetic (AF) arrangement in order to elucidate the origin of the AF–F transition. The magnetic interactions between transition metal atoms, as established from the phenomenological analysis of relating magnetic couplings and inter-atomic distances, were discussed based on the evolution of the site-decomposed density of states and the corresponding dependence of local magnetic moments on alloy composition. A satisfying agreement between experimental and calculated values of

[5] Author to whom any correspondence should be addressed.

magnetization and local magnetic moments localized on Mn, Co and Fe sites was found.

(Some figures in this article are in colour only in the electronic version)

1. Introduction

The crystal structure parameters and the magnetic properties of the $MnFe_{1-x}Co_xP$ series of solid solutions appear to be strongly correlated in the vicinity of the critical point (CP) as found in the (x, T) magnetic phase diagram (figure 1) according to the earlier work published in 1970 by Roger [1]. At this point, the Néel temperature (T_N), the Curie temperature (T_C) and the temperature of the antiferromagnetic–ferromagnetic phase transition (T_{AF-F}) are equal to each other for $x \approx 0.5$.

In the whole composition range of this system, the compounds crystallize in an orthorhombic crystal structure of the Co_2P type (space group $Pnma$). For $x < 0.5$ and $T < 250$ K the compounds exhibit AF properties only. However, for $0.5 < x < 0.8$ for each constant x two types of magnetic transition could be distinguished while increasing temperature, namely AF–F transition followed by F–P (paramagnetic) one. For $x > 0.8$ only the F–P phase transition exists.

New results on crystal structure and magnetic and electronic properties of the $MnFe_{1-x}Co_xP$ system have been recently reported by Sredniawa *et al* [2]. For $x = 0.525$, 0.65 and 0.70 the lattice parameters and atomic positions were determined by x-ray diffraction. Besides, the (P, T) magnetic phase diagram was determined for the compounds with $x = 0.45$, 0.50 and 0.525 and electronic band structure calculations were performed using the Korringa–Kohn–Rostoker (KKR) model with the coherent potential approximation (CPA) [2]. The calculated values of the magnetic moments $\mu_{tot} = 3.62\ \mu_B$/f.u. for MnFeP and $\mu_{tot} = 3.03\ \mu_B$/f.u. for MnCoP as well as the values of the hyperfine field were established. In the case of MnCoP a good agreement with the experimental values was found.

Moreover, the change of the density of states (DOS) near the Fermi level from MnFeP to MnCoP [2] tentatively explained the mechanism for the AF–F magnetic transition as detected experimentally in the investigated systems.

Noteworthily, neutron diffraction study on powder samples of MnCoP, performed by Fruchart *et al* [4], showed that magnetic structure is mostly of ferromagnetic type with however more complex behaviour at low temperatures. The values of magnetic moments ($T = 77$ K) for Mn and Co were estimated as 2.55 and 0.65 μ_B, respectively.

The magnetic structure of MnFeP was first discussed by Suzuki *et al* [5]. It was found that the compound exhibits antiferromagnetic properties with the magnetic unit cell as large as the chemical unit cell doubled along the c-axis. At 128 K the magnetic moments of the iron and manganese atoms were found to be 0.5 and 2.6 μ_B, respectively. This model of magnetic structure was not fully supported by later neutron diffraction experiments performed by Chenevier *et al* [6, 11] (see below in section 2.2.3), which yielded the following values of the magnetic moments at 4 K: 3.04 μ_B (Mn) and 0.12 μ_B (Fe).

The aim of this work was to carry out experimental investigations and establish theoretical interpretations of magnetic properties for several compositions of the $MnFe_{1-x}Co_xP$ series of compounds. Special attention was paid to the crystal lattice parameters, the atomic position parameters and the magnetic interactions between Mn, Fe and Co atoms. Besides, the influence of external magnetic field on magnetoelastic phase transitions observed in some of the compounds was studied.

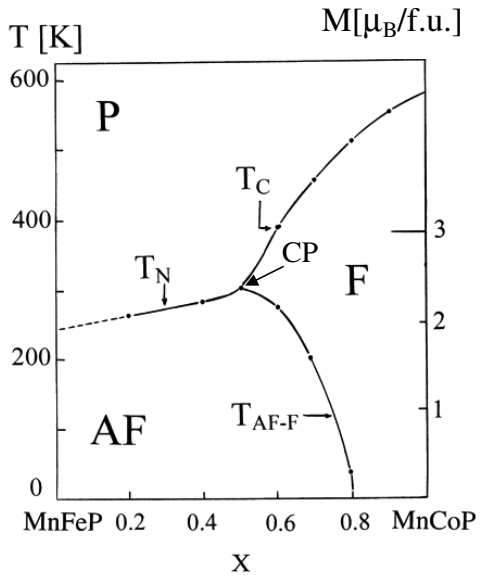

Figure 1. Magnetic (x–T) phase diagram of the orthorhombic $MnFe_{1-x}Co_xP$ (F—ferromagnetic, AF—antiferromagnetic, P—paramagnetic phase; T_N, T_C and T_{AF-F}—Néel, Curie and AF–F phase transition temperature, respectively) [1, 2].

Complementary x-ray diffraction investigations for $x = 0.3$ and high dc magnetic field experiments for $x = 0.3$, 0.45, 0.5, 0.525, 0.55, 0.65 and 0.7 are reported [3]. On this basis the parameters of crystal and electronic structure, magnetic moments and total energy were calculated in the whole range of $MnFe_{1-x}Co_xP$ composition using the KKR-CPA method within the muffin-tin approximation [7, 8]. The systematic theoretical studies enabled us to confirm the site preference of Fe/Co atoms in the series of compounds. Moreover, the variation of magnetic moments on the transition metal sublattices as well as some trends in changing DOS at the Fermi level (E_F) with the alloy composition are discussed. Electronic structure and magnetic moments of MnCoP were additionally verified by the full-potential semi-relativistic KKR computations. Moreover, different models of an AF arrangement were taken into account for the KKR-CPA calculations for the compound with $x = 0.7$ concerning the experimental results of MnFeP neutron diffraction study [5, 11] as well as the simple inter-atomic criteria for the onset of the AF/F coupling between transition metal atoms. Some correlations between exchange coupling between the Mn and Fe magnetic moments and the DOS value at E_F were noted.

2. Results and discussion

2.1. Experimental study

2.1.1. Sample synthesis. Polycrystalline samples were synthesized starting from the appropriate amount of 99.9% pure elements. The fine powders of elements were mixed, then progressively heated up to 850 °C for 8 days in evacuated silica tubes. The final heat treatment performed by high frequency heating allowed melting the sample before cooling it down. The quality of the samples was verified both by x-ray diffraction analysis as well as by magnetization measurements in weak magnetic field. X-ray diffraction experiments for the

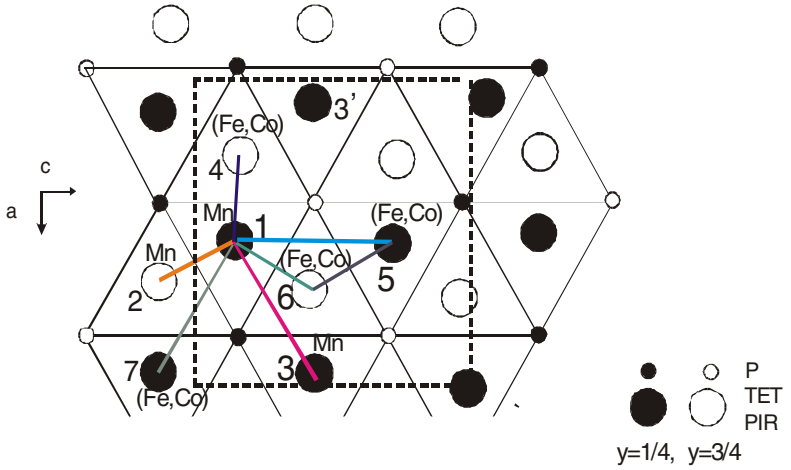

Figure 2. Interatomic distances in the orthorhombic phase for $MnFe_{1-x}Co_xP$: 1–2, the nearest (inter) Mn–Mn distances; 1–3, the nearest (intra) Mn–Mn distances; 1–4, 1–5, 1–6, the nearest (intra) Mn–(Fe, Co) distances; 1–7, the nearest (inter) Mn–(Fe, Co) distances. Symbols PIR and TET represent the atoms placed in the pyramidal (Mn) and tetrahedral (Fe, Co) sites, respectively; symbol P corresponds to the atom phosphorus.

samples were performed using a Philips diffractometer ($\lambda_{Co} = 0.1789$ nm; Bragg–Brentano geometry).

2.1.2. X-ray powder diffraction analysis. Preliminary analyses of the $MnFe_{1-x}Co_xP$ series of solid solutions were presented in [2]. The crystal structure of the orthorhombic $MnFe_{1-x}Co_xP$, as projected on the *a*–*c* plane, is shown in figure 2. X-ray diffraction was performed for the $MnFe_{1-x}Co_xP$ samples with $x = 0.525$, 0.65 and 0.7 in the temperature range 80–400 K. In this report a more detailed analysis concerning inter-atomic distances was carried out for the system.

Temperature dependences of the lattice parameters and the atomic positions (table 1) were determined using a profile refinement method. At room temperature the unit cell parameters agree fairly well with those determined earlier by Roger [1].

Neutron diffraction measurements in the paramagnetic state ($T = 320$ K) for $MnFe_{0.6}Co_{0.4}P$ and $MnFe_{0.4}Co_{0.6}P$ compounds were carried out. This technique is very suitable to analyse the atom ordering in our system, because of the large difference in the neutron scattering lengths of metals ($b_{Mn} = -3.73$ Fermi, $b_{Fe} = 9.45$ Fermi and $b_{Co} = 2.49$ Fermi). From the Bragg intensities the crystal structure was refined within the orthorhombic *Pnma* space group, where all atoms were localized in the (4c) position. We may conclude that the iron and the cobalt atoms are almost exclusively placed in the tetrahedral sites and the manganese atoms in the pyramidal sites only. The refinements give no evidence that there is important deviation from stoichiometry either in the metal atom or in the non-metal atom sublattice. However, it should be noted, that a very slight lack of absolute metal atom ordering (about 1%) was detected.

The thermal behaviour of the unit cell parameters reveals the magnetoelastic character of $MnFe_{0.7}Co_{0.3}P$ at T_N as shown in figure 3. The corresponding change of the unit cell volume is $\Delta V/V \sim 0.11\%$.

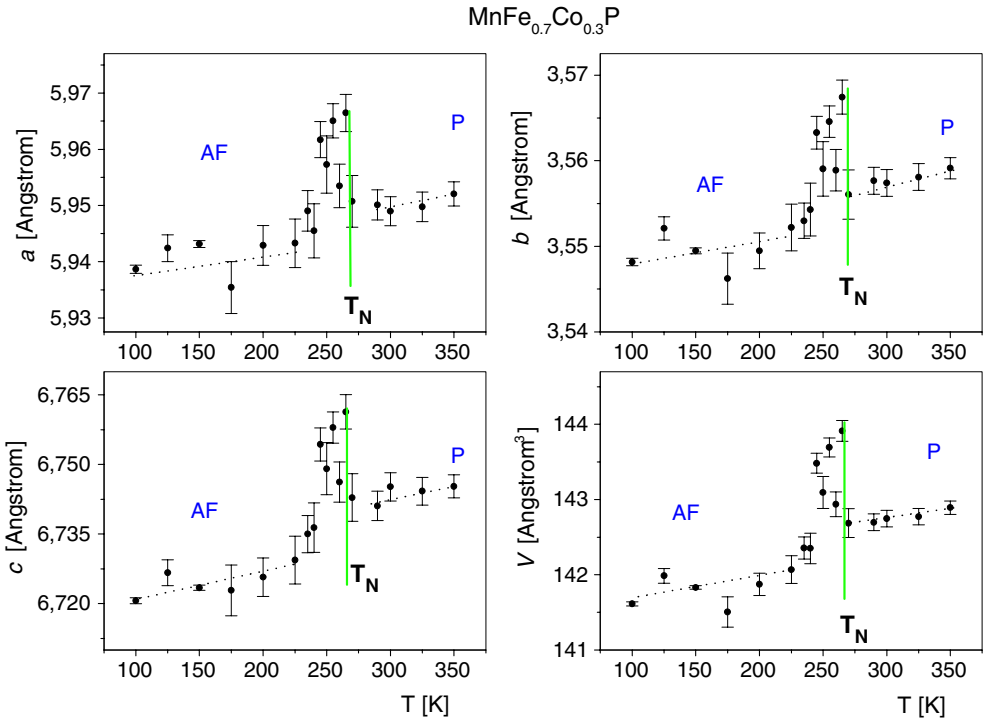

Figure 3. Thermal dependence of the a, b, c lattice parameters and the unit volume V for $MnFe_{0.7}Co_{0.3}P$ [3]. AF—antiferromagnetic phase, P—paramagnetic phase, T_N—Néel temperature as determined earlier in [1, 2].

Table 1. Lattice parameters and atomic positions at 100 K refined for the samples with $x = 0.3$, 0.525, 0.65 and 0.7 cobalt content [3].

Lattice parameters	Composition			
	$x = 0.3$	$x = 0.525$	$x = 0.65$	$x = 0.70$
	$T = 100$ K			
a (Å)	5.9396(7)	5.940(2)	5.930(3)	5.932(3)
b (Å)	3.5482(4)	3.542(1)	3.520(2)	3.517(2)
c (Å)	6.7206(6)	6.725(3)	6.710(4)	6.720(3)
V (Å^3)	141.61(3)	141.52(9)	140.10(14)	140.21(11)
$x_{Co,Fe}$, $z_{Co,Fe}$	0.858(2), 0.064(1)	0.850(2), 0.056(2)	0.851(2), 0.063(9)	0.846(2), 0.063(2)
x_{Mn}, z_{Mn}	0.979(2), 0.671(1)	0.969(2), 0.669(2)	0.972(2), 0.067(2)	0.968(2), 0.667(2)
x_P, z_P	0.232(3), 0.126(2)	0.232(3), 0.118(2)	0.235(4), 0.127(2)	0.233(4), 0.123(2)

For all the compounds exhibiting AF ordering at low temperatures, a change in the lattice parameters has been observed when the AF ordering takes place. For samples with $0.3 < x < 0.7$ the lattice parameters decrease abruptly in the vicinity of the AF–P, AF–F and F–P phase transitions. No change of the crystallographic space group was found to be associated with this drop. Simultaneously, it was established that the relative drop of the unit cell volume occurring at the F–P transition slightly decreases when the cobalt content increases.

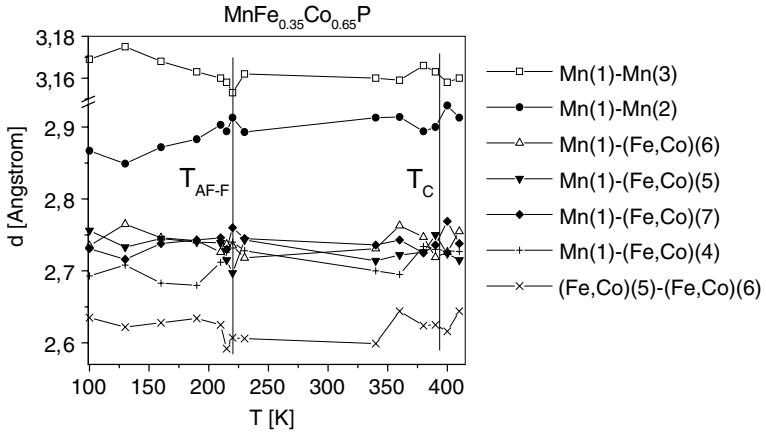

Figure 4. Temperature dependence of the inter-atomic distances for $MnFe_{0.35}Co_{0.65}P$ [3].

Table 2. The interatomic distances for $MnFe_{0.35}Co_{0.65}P$ at different temperatures (F—ferromagnetic, AF—antiferromagnetic, P—paramagnetic phase, cr—the critical distance between transition metal atoms for the onset of the F/AF coupling) [3].

T (K)	State	Mn–P (Å)	(Fe, Co)–P (Å)	Mn–Mn (Å)		Mn–(Fe, Co) (Å)			(Fe, Co)–(Fe, Co) (Å)
100	AF	2.56_9 2.49_1 2.39_8	2.31_1 2.21_8 2.21_6	3.16_9 AF 2.86_7 cr	2.75_6 cr	2.73_5 cr	2.69_3 cr	2.72_7 cr	2.63_5
130	AF	2.42_2 2.48_5 2.56_5	2.20_5 2.22_8 2.29_5	3.17_5 AF 2.84_9 cr	2.73_3	2.76_5	2.70_8	2.71_6	2.62_2
190	AF	2.47_7 2.57_1 2.49_3	2.21_3 2.22_4 2.22_2	3.16_3 AF 2.88_3 cr	2.74_0	2.74_2	2.68_0	2.74_3	2.63_4
360	F	2.46_3 2.49_4 2.54_3	2.16_1 2.25_7 2.33_6	3.15_9 AF 2.91_4 cr	2.72_2	2.76_3	2.69_5	2.74_3	2.64_4
410	P	2.71_5 2.75_5 2.72_7	2.19_4 2.32_1 2.24_9	3.16_0 AF 2.91_3 cr	2.71_5	2.75_5	2.72_7	2.73_8	2.64_4
Numbers of atoms refer to figure 2.				1–3 1–2	1–5	1–6	1–4	1–7	5–6

For the sample with $x = 0.65$ changes of the interatomic distances between the metal atoms were derived in the vicinity of both the AF–F (∼210–215 K) and the F–P (∼390–400 K) phase transition (figure 4). In particular, the largest changes of the interatomic distance were observed (table 2) for the Mn(1)–Mn(2) and Mn(1)–(Fe, Co)(5) pairs of atoms (referenced to figure 2), whereas the jumps were found to be weaker for the Mn(1)–(Fe, Co)(4), Mn(1)–(Fe, Co)(7), Mn(1)–(Fe, Co)(6), (Fe, Co)(7)–(Fe, Co)(6) and Mn(1)–Mn(3) pairs.

2.1.3. High dc field magnetization measurements. The aim of the measurements was to determine the influence of high magnetic field on the critical point in the (x, T) phase diagram,

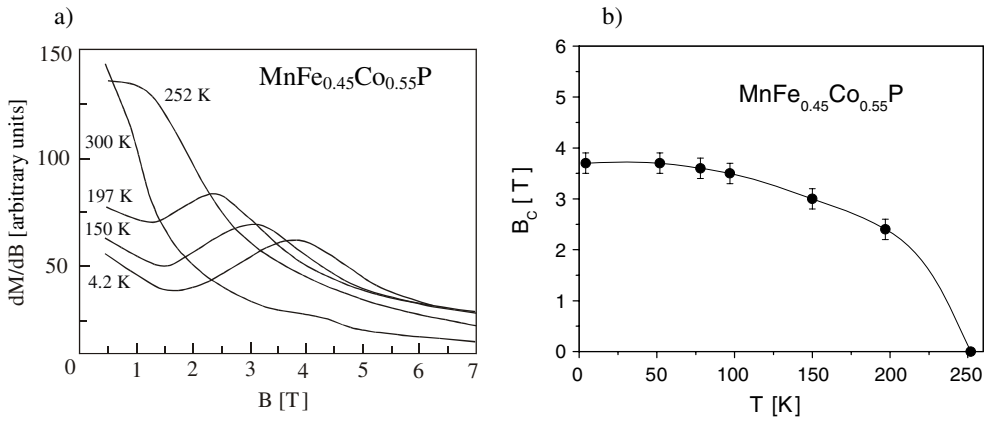

Figure 5. (a) Derivative of magnetization dM/dB for $MnFe_{0.45}Co_{0.55}P$ [3]. (b) Thermal variation of the transition field for $MnFe_{0.45}Co_{0.55}P$ [3].

especially to see whether any field induced magnetic phase transition can be found in the $MnFe_{1-x}Co_xP$ system. The magnetic properties of the compounds with $x = 0.3$, 0.45, 0.5, 0.525, 0.55, 0.65, 0.7 and 0.8 were systematically investigated in magnetic fields up to 20 T at LCMI, Grenoble.

Two types of experiments were carried out: either iso-thermal $M_T(B)$ or iso-field $M_B(T)$ data sets were collected. In both cases the scenario of the experiment is detailed hereafter. Before the first experiment or after each half cycle (increasing and decreasing field) the samples were heated above the ordering temperature (≈20 K) and then cooled down to the desired temperature (in zero field—i.e. ZFC process).

The results for the compounds with low Co content, i.e. $x = 0.3$ and 0.45, are presented first. The $M_T(B)$ curves reveal that the AF ordering was stabilized in both compounds for fields up to 20 T and for temperatures up to 250 K. So, for $MnFe_{0.7}Co_{0.3}P$, the variation of the dM/dB derivative versus B at 4.2 K exhibits only a weakly marked maximum for fields about 5 T. Very similar trends were found for $MnFe_{0.55}Co_{0.45}P$.

For the intermediate cobalt content, namely for $MnFe_{0.45}Co_{0.55}P$ and $MnFe_{0.475}Co_{0.525}P$, more interesting trends were evidenced from $M_T(B)$ curves. Figures 5 and 6 present the $M_T(B)$ traces obtained for both compounds at different temperatures. A special behaviour was found for a critical field ranging to 4 T as shown in figure 5(a). A similar kink was also deduced from all the magnetization curves recorded up to 300 K as shown in figure 5(b). For $MnFe_{0.475}Co_{0.525}P$ the $M_T(B)$ curves reveal that the magnetic behaviour exhibits a similar anomaly (figure 6). For both compounds, with $x = 0.525$ and 0.55, the critical field corresponding to such kinks was found to decrease when temperature increases.

For compounds having the largest cobalt content ($x \geqslant 0.65$) the $M_T(B)$ curves are typical for nearly ferromagnetic systems, similar to the MnCoP parent compound as found by Roger [1] and latter reported in [3] and [4]. This type of behaviour will not be discussed here because of the absence of field induced magnetic transformation.

No magnetic field hysteresis was observed for the magnetic field induced phase transitions ($x = 0.525$, $x = 0.55$) and no temperature hysteresis in the temperature dependence of the ac susceptibility was detected within the experimental accuracy [2, 3]. Finally, the above conclusions were also supported by the x-ray diffraction experiments. They showed that in the case of the magnetoelastic phase transitions no temperature hysteresis was established in the vicinity of the phase transformation.

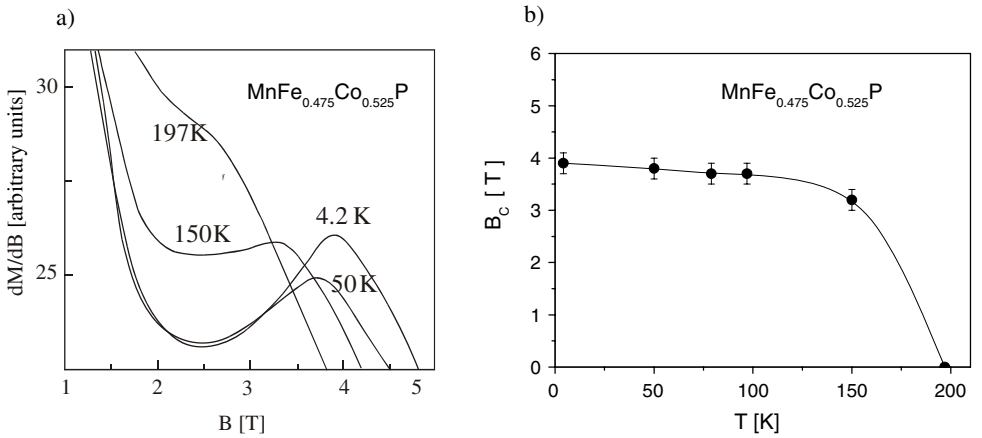

Figure 6. (a) Derivative of magnetization dM/dB for $MnFe_{0.475}Co_{0.525}P$ [3]. (b) Thermal variation of the transition field for $MnFe_{0.475}Co_{0.525}P$ [3].

Table 3. KKR-CPA total energy for disordered $Mn_{1-y}Fe_yCoP$ [E^{Mn}(imp)] and $MnCo_{1-y}Fe_yP$ [E^{Co}(imp)] systems, when diluting Fe impurity on the Mn or Co site, respectively. This is compared to E^{Co}(vac) and E^{Mn}(vac) obtained in the $Mn_{1-y}CoP$ and $MnCo_{1-y}P$ systems containing vacancies. $\Delta E^{Co} = E^{Co}(imp) - E^{Co}(vac)$ and $\Delta E^{Mn} = E^{Mn}(imp) - E^{Mn}(vac)$ represent the corresponding differences. All values are given in Ryd.

	Co site			Mn site		
y	E^{Co}(imp)	E^{Co}(vac)	ΔE^{Co}	E^{Mn}(imp)	E^{Mn}(vac)	ΔE^{Mn}
0.005	−22 948.640	−22 898.168	−50.472	−22 957.904	−22 907.435	−50.469
0.015	−22 939.122	−22 787.708	−151.414	−22 966.913	−22 815.508	−151.405
0.05	−22 905.808	−22 401.102	−504.706	−22 998.445	−22 493.766	−504.679

2.2. Theoretical study

2.2.1. Site preference. The question of site preference of Fe diluted in MnCoP was addressed to total energy KKR-CPA computations. Bearing in mind that the atomic coordinations of two transition metal atoms are different, the analysis of differences in total energy (E_{tot}) of the Fe impurity diluted either on Co or Mn positions seems to be interesting due to the proximity of these atoms in the periodic table. Since the Fe impurity acts either as an electron donor (Mn site) or as an electron acceptor (Co site), the direct E_{tot} comparison of $MnCo_{1-y}Fe_yP$ and $Mn_{1-y}Fe_yCoP$ is useless due to different numbers of electrons in the two systems. Similarly, the comparison of the formation energy (the balance between the LDA total energy of the solid and the sum of the constituent atom energies) informs us about the relative crystal stability of structures, but the selective substitution of the element cannot be decided. Hence, it was necessary to use a more convincing criterion of the site preference in these systems. We have referred the total energies of $MnCo_{1-y}Fe_yP$ and $Mn_{1-y}Fe_yCoP$ alloys to those obtained in $MnCo_{1-y}P$ and $Mn_{1-y}CoP$ (containing the same concentration of vacancy defects). The resulting energy differences, i.e. $\Delta E^{Co} = E_{tot}(MnCo_{1-y}Fe_yP) - E_{tot}(MnCo_{1-y}P)$ and $\Delta E^{Mn} = E_{tot}(Mn_{1-y}Fe_yCoP) - E_{tot}(Mn_{1-y}CoP)$, were then compared for several y contents. The smaller value between ΔE^{Mn} and ΔE^{Co} indicates the site preference, since E_{tot} of the system decreases more when an Fe impurity substitutes the atom occupying this site. Table 3 presents the KKR-CPA results obtained at three illustrative y concentrations. One observes

that ΔE^{Co} is smaller than ΔE^{Mn}, and the discrepancy between the two values increases with y. Our result clearly proves that substituting Co with Fe on the tetrahedral site is much more favourable than substituting Mn on the pyramidal site. This is in excellent agreement with the experimental observations that Fe occupies exclusively tetrahedral sites in $MnFe_{1-x}Co_xP$ [10]. Noteworthily, the Fe impurity diluted on the unfavourable Mn sites in MnCoP should carry markedly larger magnetic moment (2.4 μ_B) than the one on the preferred Co sites (0.6 μ_B), which is in contradiction with the experiments [5, 11].

2.2.2. Ferromagnetic state of $MnFe_{1-x}Co_xP$. The band structure of orthorhombic MnCoP and MnFeP parent compounds shows [2] that similarly as in other MnMX compounds [9] the local magnetic moment located on pyramidal sites (Mn) is considerably larger than that on the tetrahedral sites (Co and Fe). Considering ferromagnetic ordering, which is almost the case for MnCoP [4], the calculated magnetic moment of Fe (0.55 μ_B) is twice that of Co (0.28 μ_B), whereas the Mn magnetic moment is almost the same (about 2.7–2.9 μ_B) in both compounds.

In our previous paper [2] the electronic structure for the $MnFe_{1-x}Co_xP$ ($x = 0.525$) compound was discussed. The calculated ^{57}Fe hyperfine field (Fermi contact contribution) was successfully compared with Mössbauer spectroscopy results. Hence, it was interesting to undertake more systematic electronic structure calculations to enlighten the origin of the AF–F transition occurring in the $MnFe_{1-x}Co_xP$ series. Special attention was paid to evolution of local magnetic moments on transition metal atoms as well as DOS modifications near the Fermi level.

The KKR method with coherent potential approximation (CPA) [7, 8] within the LDA framework and muffin-tin crystal potential have been used to calculate the total, site-decomposed and l-decomposed DOS as well as total magnetization and local magnetic moments on constituent atoms. The experimental values of crystal structure parameters (table 1 and references [2, 3]) have been used in all our computations. In the case of ferromagnetic MnCoP the previous muffin-tin KKR results have been verified by full potential semi-relativistic KKR calculations, that converged to magnetic moments ($\mu_{Mn} = 2.88\ \mu_B$, $\mu_{Co} = 0.29\ \mu_B$) which are in good agreement with the previous results [2] and neutron diffraction data ($\mu_{Mn} = 2.55\ \mu_B$, $\mu_{Co} = 0.65\ \mu_B$ [4] and $\mu_{Mn} = 2.66\ \mu_B$, $\mu_{Co} = 0.06\ \mu_B$ [15]). Noteworthily, the saturation magnetization measured for MnCoP is as large as 3.2 μ_B, which agrees fairly well with both theoretical derivation and experimental data [4].

The corresponding total and site-decomposed DOSs in MnCoP are shown in figure 7. There is a deep minimum of DOS clearly visible near the Fermi level which arises from strong hybridization of d states of Mn and Co (a 'pseudogap' behaviour). This electronic structure feature can be better visualized by dispersion curves (figure 8), in which an energy gap appears all along most of the high symmetry directions in the orthorhombic Brillouin zone.

Figure 9 (low panel) presents the concentration dependence of total and local magnetic moments in $MnFe_{1-x}Co_xP$ assuming the ferromagnetic state. One notices that magnetic moments on Mn (about 2.9 μ_B) and Co (0.25 μ_B) remain almost constant while changing x, whereas μ_{Fe} decreases from 0.83 μ_B ($x = 0$) to 0.56 μ_B ($x = 1$). This behaviour results in the decrease of the total magnetization from 3.6 μ_B ($x = 0$) to about 3.1 μ_B ($x = 1$) due to substitution of Co for Fe. Our results can be compared with experimental data only for Co rich samples, i.e. $0.8 < x < 1.0$, where ferromagnetic ordering appears effectively. Indeed, the calculated magnetization ($\sim$3.1 μ_B) agrees well with the measured magnetization of $MnFe_{0.2}Co_{0.8}P$ [1, 3].

The analysis of DOS near E_F sheds light on reasons for changing magnetic structure (from F to AF) when the Fe concentration increases. Figure 9 shows the concentration dependence of $N_{tot}(E_F)$ ($N_{tot}(E_F) = N_+(E_F) + N_-(E_F)$). In spite of small changes in values of the

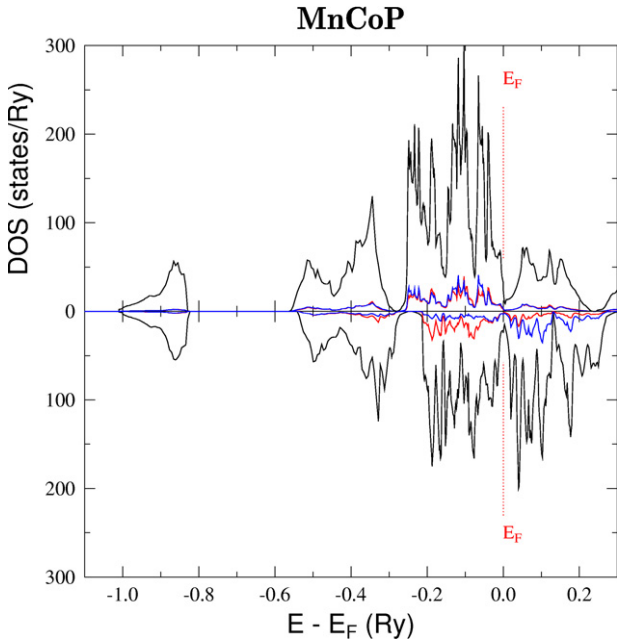

Figure 7. Density of states in orthorhombic MnCoP. Total DOS and Mn and Co contributions are plotted black, blue (dark) and red (light), respectively. The Fermi level is at zero (marked by a vertical line).

local magnetic moments with the alloy composition, the total DOS drastically increases, from ∼9 states/Ry/f.u. for MnCoP to ∼33 states/Ry/f.u. for $MnFe_{0.2}Co_{0.8}P$. This is mainly due to a significant increase of DOS on the Fe site. At the same time, the increase of the corresponding Mn and Co contributions is much smaller. The KKR-CPA electronic structure behaviour of $MnFe_{1-x}Co_xP$ suggests that for high Co contents ($0.8 < x < 1$) the ferromagnetic state is energetically favourable due to low $N(E_F)$. But with increasing Fe concentration a strong enhancement of $N(E_F)$ seems to drive the system to a more advantageous magnetic state and is likely responsible for the observed F–AF transition. These trends in electronic structure behaviours are well seen in figure 10, where the spin-polarized DOS of $MnFe_{0.3}Co_{0.7}P$ (computed in F state) is presented. In this case, the Fermi level falls into the high DOS peak for spin-down electrons and it is located on the strongly increasing DOS slope for spin-up electrons.

2.2.3. AF–F transition in $MnFe_{1-x}Co_xP$. The KKR-CPA calculations assuming different AF structures were performed in the case of $MnFe_{0.7}Co_{0.3}P$. On the whole, these computations support trends to decrease $N(E_F)$ in the AF state with respect to the F one. Neutron diffraction investigations [5, 11, 13] report that the magnetic structure of MnFeP is rather complex and can be approximately described as a c-axis doubled cell ($c' = 2c$) of the orthorhombic chemical one. But in the papers above the authors refined various values of the local magnetic moments on Mn and Fe as well as proposing different magnetic structures. Later, Sjöstrom *et al* [14] showed that the ^{57}Fe Mössbauer spectra of MnFeP at low temperature can be explained by a modulated magnetic structure described by a linear combination of an AF and a helical mode, which agrees with neutron diffraction results of Chenevier [11]. Nevertheless, we consider that

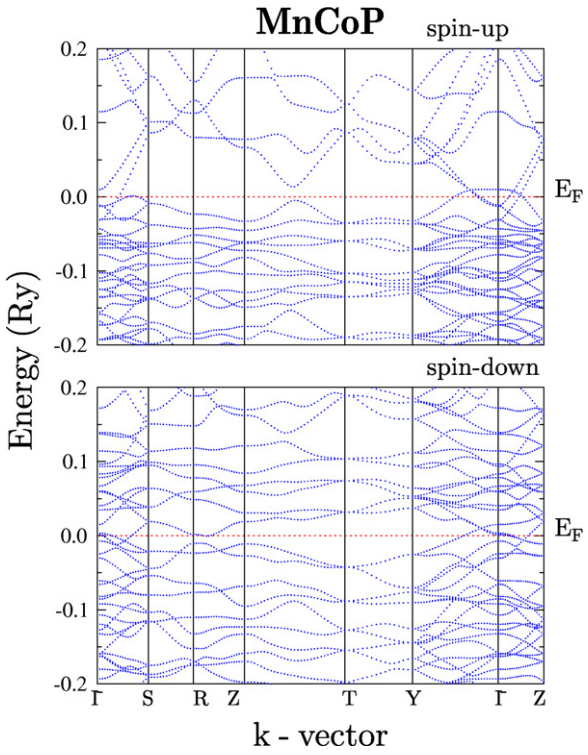

Figure 8. KKR dispersion curves $E(\mathbf{k})$ in the orthorhombic MnCoP for spin-up (left) and spin-down electrons. The energy gap near E_F (marked by a horizontal red line) is observed along most BZ directions.

collinear components approximate rather well the magnetic structure as described by a c-axis doubled cell.

As shown in this work, the coupling between (Fe, Co) and Mn in $MnFe_{1-x}Co_xP$ ($x > 0.5$) strongly depends on the Mn–Mn and Fe–Mn distances. The choice of possible AF couplings in the theoretical investigations was partly inspired by previously reported neutron diffraction data as well as the simple inter-atomic distance criteria for magnetic coupling between transition elements [4, 12].

Bearing in mind that the present KKR-CPA calculations allow us to treat only parallel alignment of magnetic moments (coupled either F or AF) a few models have been considered. The coupling via the shortest inter-atomic distances (see figure 2) Mn(1)–Mn(2), (Fe, Co)(5)–(Fe, Co)(6) and Mn(1)–(Fe, Co)(4) was taken to be either F or AF (see table 4). Except model I corresponding to the simple ferromagnetic state, in all the other models (different types of AF) the magnetic moments on Mn and (Fe, Co) atoms are considered to couple in such a way that they result in zero magnetization per c-doubled cell. Three examples of the considered AF models are depicted in figure 11. Although the magnetic structures, as mentioned in table 4, do not cover all possible configurations, the comparison of the most plausible cases enables us to study the effect of the magnetic coupling on the electronic structure (especially in the vicinity of the Fermi level) as well as on the local magnetic moments.

The KKR-CPA results of Mn, Fe and Co magnetic moments as well as the total DOS at E_F (per f.u.) are collected in table 5. We can conclude that small magnetic moments on tetrahedral

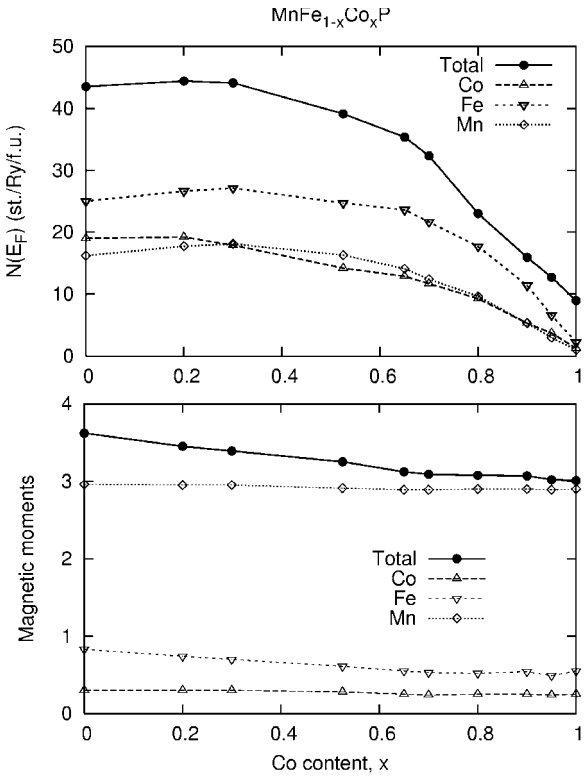

Figure 9. Concentration dependence of the total and the site-decomposed DOS at E_F (upper panel), the total (per f.u.) and the local magnetic moment (lower panel) in $MnFe_{1-x}Co_xP$ (magnetic moments in μ_B).

Table 4. Considered models of magnetic coupling (F and AF) between transition metal elements in $MnFe_{0.7}Co_{0.3}P$. Mn–Mn (inter) and Mn–Mn (intra) represent the shortest distances between the Mn atoms between and within the *a*–*c* planes, respectively. The next columns correspond to the shortest distances between Mn and (Fe, Co) atoms, namely Mn–(Fe, Co) (inter) and Mn–(Fe, Co) (intra), see text.

Magnetic structure model	Mn–Mn (inter)	Mn–Mn (intra)	Mn–(Fe, Co) (inter)	Mn–(Fe, Co) (intra)
Model I	F	F	F	F
Model II	AF	F	F	F/AF
Model III	AF	AF	F/AF	F/AF
Model IV	AF	F	AF	AF
Model V	F	AF	F/AF	F/AF

sites (occupied by Fe or Co) are very sensitive to the type of magnetic coupling. The calculated moment on Fe varies from ∼0.7 to ∼0.3 μ_B depending on the magnetic structure model, and in the case of Co it may even disappear (model III). Conversely, the magnetic moment on Mn seems to be not affected by variable inter-atomic distances (see figure 10) or by the type of magnetic coupling (table 5) and it was found to be ∼2.95 μ_B.

Taking into account that the analysis of DOS value at the Fermi level $N(E_F)$ is in general an insufficient criterion for stability of a magnetic state, one can, however, try to find out some

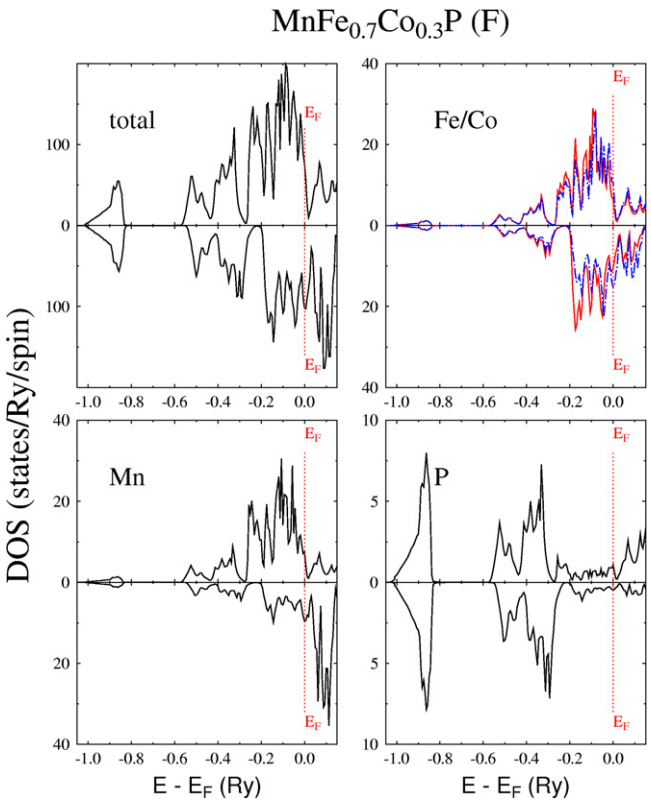

Figure 10. KKR-CPA density of states in $Mn_{0.3}Fe_{0.7}CoP$ in the ferromagnetic state. The total DOS and the Mn and Co contributions are plotted in separate panels. Fe and Co located at the tetrahedral site are represented by blue (dot–dashed) and red (solid) curves, respectively. The Fermi level is at zero (marked by a vertical line).

Table 5. Local and total (per unit cell) magnetic moments and the atomic DOS at E_F in $MnFe_{0.7}Co_{0.3}P$ for different types of magnetic structure (see table 3).

Magnetic structure model	Magnetic moments (μ_B)			DOS at E_F (states/Ryd)			
	Mn	Fe	Co	Total	Mn	Fe	Co
Model I	2.94	0.70	0.30	168	17.3	26.1	16.9
Model II	2.92	0.56	0.22	135	13.1	24.8	11.5
Model III	2.94	0.32	0.07	137	14.1	20.2	14.9
Model IV	2.95	0.42	0.07	156	15.6	23.9	17.7
Model V	2.95	0.50	0.17	206	23.3	24.1	18.3

trends as seen from KKR-CPA computations of AF $MnFe_{0.7}Co_{0.3}P$. Table 5 shows that the most stable antiferromagnetic structure may correspond to models II and III, in which the AF coupling appears between the Mn atoms in the parallel $[0, 1/4, 0]$ and $[0, -1/4, 0]$ planes where the inter-atomic distances are the shortest. This magnetic coupling seems to be crucial for minimizing DOS at E_F, whereas the coupling between the Mn atoms in the same a–c plane is expected to be less important. The second reason for lowering DOS at E_F (see figure 12 for detailed site-dependent DOS contributions) is presumably related to ferromagnetic coupling

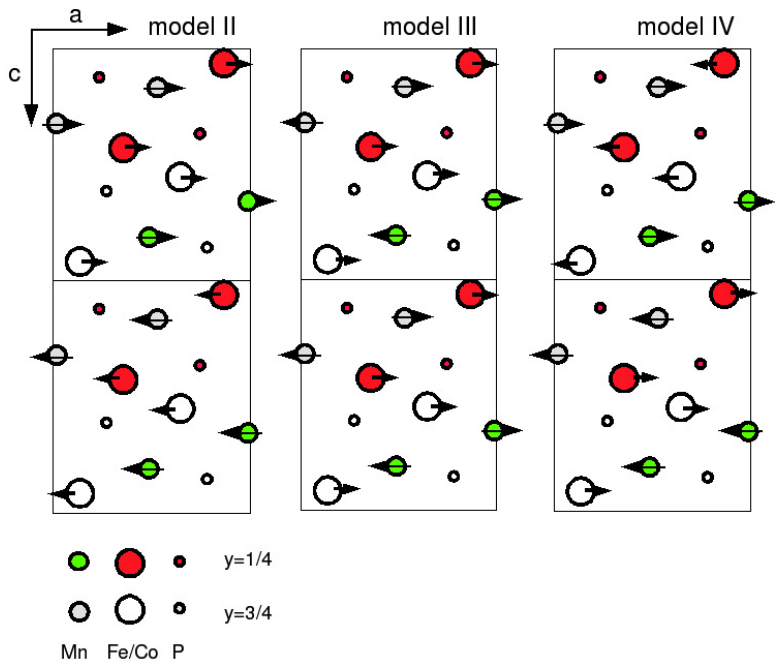

Figure 11. The illustrative AFM structure models (II, III and IV) used in the KKR-CPA computations (see also table 4).

between (Fe, Co) and Mn atoms in the parallel a–c planes, called Mn–(Fe, Co) (intra). This F coupling is realized in model II, for which the lowest value of $N(E_F)$ was calculated. In the case of model III (also admissible due to comparably low $N(E_F)$), the coupling between Mn and NN (Fe, Co) can be either F or AF. On the other hand, the F coupling between the Mn atoms separated by the shortest inter-atomic distances (Mn–Mn inter), found in model V, is highly unfavourable, due to high DOS values on all these atoms. In order to support our analysis based uniquely on the DOS characteristics in the vicinity of the Fermi level, the total energy in the three AF models of $MnFe_{0.7}Co_{0.3}P$ was calculated. E_{tot} of model II, which equals $-44\,574.129$ Ryd (per c-doubled cell), was found to be $\sim$15 and $\sim$60 mRyd below the values obtained for models IV and V, respectively. This result supports the conclusion that the AF magnetic structure with the lowest energy (model II) also exhibits the smallest value of DOS at E_F.

It is worthwhile to point out that any prior selection of magnetic coupling between the Mn atoms (inter and intra) makes establishing a simple coupling between Mn and (Fe, Co) rather difficult (or even impossible), since in our computations (by limiting possible angles between magnetic moments) we allow only for either parallel or anti-parallel alignment of magnetic moments. Such models cannot describe physically interesting behaviour of spin frustration, which is likely to be present in the $MnFe_{0.7}Co_{0.3}P$ system, as can be expected from the neutron diffraction and the Mössbauer spectroscopy measurements in the MnFeP compound. One can find it interesting that the magnetic structure types (models II and III) resulting in the lowest DOS at E_F can be roughly seen as the border cases of the experimentally determined magnetic structure of MnFeP [11]. Hence, we expect that our analysis based on the $N(E_F)$ criterion has provided a valuable insight into the microscopic origin of the complex magnetic behaviour observed in the $MnFe_{1-x}Co_xP$ system. The trends in KKR-CPA DOS

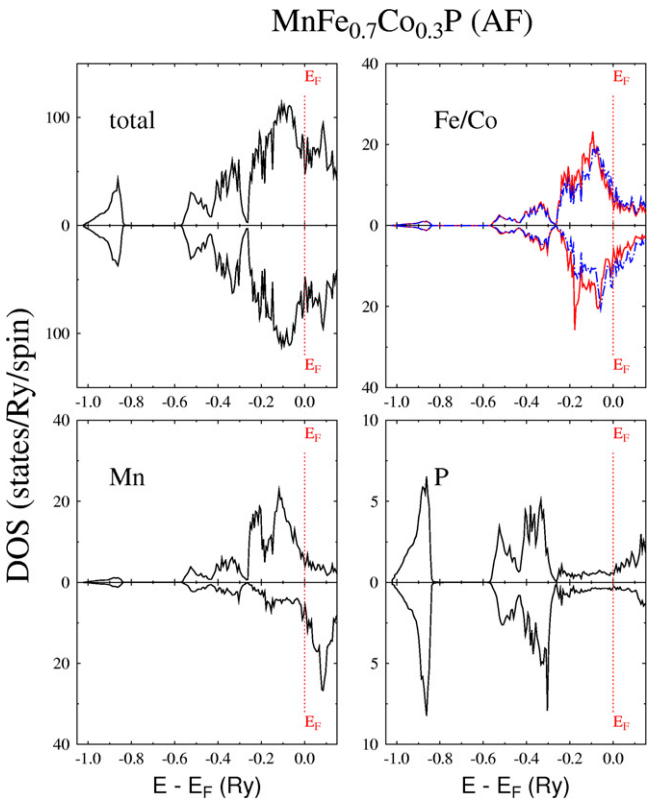

Figure 12. KKR-CPA density of states in $Mn_{0.3}Fe_{0.7}CoP$ in the ferromagnetic state. The total DOS and the Mn and Co contributions are plotted in separate panels. Fe and Co located at the tetrahedral sites are represented by blue (dot–dashed) and red (solid) curves, respectively. The Fermi level is at zero (marked by a vertical line).

variations versus type of magnetic coupling can be compared with simple criteria established for transition metal atoms, which relate F/AF coupling to inter-atomic distances [4, 12]. The magnetic interactions in intermetallic compounds are often discussed on the basis of criteria related to the metal atom separation. There are several rules which allow us to classify different types of magnetic interactions. For Mn–Mn and for Fe–Fe a critical separation distance of 2.8 and 2.6 Å, respectively, was introduced. In the case of our system these criteria are confirmed and remain in agreement with our band structure analysis.

3. Conclusions

The above presented crystal, magnetic and electronic structure systematic characterizations of the $MnFe_{1-x}Co_xP$ series of compounds have enabled us to deduce and summarize some general features of this system. Firstly, magnetic field induced phase transitions were observed for $x = 0.55$ and 0.525 contents only. The critical field for which the transition occurs was found to decrease versus temperature. Secondly, a magnetoelastic phase transition was found to occur at T_N. Significant changes of all the lattice parameters as well as the unit cell volumes were found. The magnetoelastic effect and the field induced transformations result from a strong competition of exchange forces between different 3d metal sites. A critical

situation occurs when about half of the Fe atoms are substituted by Co ones. Thirdly, the magnetic couplings between Mn, Fe and Co atoms for selected $MnFe_{1-x}Co_xP$ compounds were discussed. Fourthly, the magnetic interactions among transition metal atoms, as established from the above mentioned phenomenological analysis relating magnetic coupling and inter-atomic distances, agree with the evolution of site-decomposed DOS and the corresponding local magnetic moments. In particular, the KKR-CPA total energy analysis well supported the preference of the tetrahedral Co site for the Fe impurity introduced into MnCoP.

The electronic structure calculations of $MnFe_{1-x}Co_xP$ showed also that the disappearance of the AF state and the tendency to form the F state while increasing Co concentration are related to a strong decrease in the total DOS at E_F for $x > 0.6$. Interestingly, a significant drop in $N(E_F)$ is associated with only slight changes in magnetic moments.

In MnCoP the Fermi level falls into a 'pseudogap' separating the valence and the conduction band, which suggests interesting electron transport properties. The magnetic moments calculated for MnCoP are in good agreement with the neutron diffraction data.

In the case of $MnFe_{0.7}Co_{0.3}P$, the KKR-CPA computations assuming different AF models were performed. They revealed that AF coupling between Mn–Mn (inter) plays a predominant role to decrease $N(E_F)$ with respect to the F coupling. Nevertheless, the magnetic coupling for the shortest Mn–(Fe, Co) (inter) distances also seems to be important for stability of the magnetic state. Noteworthily, the type of magnetic coupling practically does not affect the value of the Mn magnetic moment ($\sim$2.95 μ_B), whereas small magnetic moments on Fe and Co atoms were found to be very sensitive to both inter-atomic distances between transition metals as well as to the type of magnetic coupling.

Neutron diffraction experiments on $MnFe_{1-x}Co_xP$ are in progress to verify the existence of the most favourable magnetic ordering types from the AF models suggested on the basis of the electronic structure computations.

Acknowledgments

Financial support from the Ministry of Education and Science through grant No. 1 P03B 113 29 is gratefully acknowledged. This work was also partly supported by the French–Polish cooperation project (Polonium).

References

[1] Roger A 1970 *PhD Thesis* University of Paris-Orsay
[2] Średniawa B, Zach R, Fornal P, Duraj R, Bombik A, Tobola J, Kaprzyk S, Nizioł S, Fruchart D, Bacmann M, Fruchart R and Stanek J 2001 *J. Alloys Compounds* **317/318** 266
[3] Średniawa B 2003 *PhD Thesis* AGH Kraków
[4] Fruchart D, Martin-Farrugia C, Rouault A and Sénateur J P 1980 *Phys. Status Solidi* a **57** 675–82
[5] Suzuki T, Yamaguchi Y, Yamamoto H and Watanabe H 1973 *J. Phys. Soc. Japan* **34** 911
[6] Fruchart D, Bacmann M and Chauduet P 1980 *Acta Crystallogr.* B **36** 2759
[7] Bansil A, Kaprzyk S, Mijnarends P E and Tobola J 1999 *Phys. Rev.* B **60** 13396
[8] Stopa T, Kaprzyk S and Tobola J 2004 *J. Phys.: Condens. Matter* **16** 4921
[9] Fujii S, Ishida S and Asano S 1988 *J. Phys. F: Met. Phys.* **18** 971
[10] Fruchart R 1982 *Ann. Chim. Fr.* **7** 563
[11] Chenevier B 1990 *PhD Thesis* Université J Fourier, Grenoble
[12] Yamada T, Kunitomi N and Nakai Y 1970 *J. Phys. Soc. Japan* **28** 615
[13] Bacmann M *et al* 2007 at press
[14] Sjöström J, Häggström L and Sundqvist T 1988 *Phil. Mag.* B **57** 737
[15] Fujii H, Komura S, Takeda T, Hokabe T and Okamoto T 1979 *J. Magn. Magn. Mater.* **14** 181